International Conference on Deep Excavations
28-30 June 2006, Singapore

Nicoll Highway Collapse: Evaluation of Geotechnical Factors Affecting Design of Excavation Support System

A.J. Whittle, *Massachusetts Institute of Technology, Cambridge, MA, USA*,
R.V. Davies, *Benaim (UK), Bath, UK*,

ABSTRACT: This paper summarizes the site characterization, selection of soil parameters and analyses of soil-structure interaction that affected the design of the support system for the Circle Line Stage 1 excavations at contract C824, adjacent to the Nicoll Highway. Features of the local stratigraphy included a buried channel in the underlying Old Alluvium which affected directly the installation of perimeter diaphragm wall panels. Surface settlements and pore pressures measured prior to construction strongly suggest on-going consolidation of the Marine Clay due to land reclamation in the 1970's. From the evidence available, the Authors concluded that the lower Marine Clay unit was underconsolidated resulting in a relatively low undrained shear strength of the clay in relation to the total overburden pressure. Uncertainties existed in drainage conditions in the Old Alluvium and despite extensive post-failure investigations, the installed locations, behavior and mass properties of jet grout pile-rafts remain highly uncertain. The original analysis of soil-structure interaction was carried out using nonlinear finite element methods with linearly-elastic, Mohr-Coulomb (MC) models to represent the soil behavior. The use of this soil model together with drained effective stress strength parameters (c', ϕ'), in an undrained setting, greatly overestimated the undrained shear strength of the Marine Clay in the original design leading to a serious underestimation of computed wall deflections, bending moments and the mobilization of forces in the JGP pile-rafts.

1 INTRODUCTION

The government of Singapore has acted quickly to investigate the causes and contributory factors leading to the collapse of the Nicoll Highway on April 20th 2004. The Committee of Inquiry report (COI, 2005) identified two key errors in the design of the temporary lateral earth support system for the adjacent excavation of the Circle Line, contract C824: 1) under-design of the diaphragm wall due to the method of analyzing soil-structure interaction; and 2) under-design of the waler connections in the strutting system. The Authors contributed to the Committee of Inquiry as experts appointed by LTA. This paper reviews the geotechnical factors leading to the under-design of the diaphragm wall.

Figure 1 illustrates the original design of the lateral earth support system in the area where the collapse initiated (type M3, Fig. 2). The construction involved a 33.3m deep, cut-and-cover excavation which is approximately 20m wide. The excavation support system includes 0.8m thick diaphragm walls which extend through deep layers of Estuarine and Marine clays (Kallang formation) and are embedded a minimum of 3m within the underlying Old Alluvium (layer SW-2). The walls are supported by a total of ten levels of pre-loaded, cross-lot bracing and by two rafts of continuous Jet Grout Piles (JGP). The Upper JGP raft is a sacrificial layer that is excavated after installation of the 9th level of struts. Collapse occurred on April 20th 2004 following excavation of the Upper JGP (to an elevation of approximately 72.3m RL, Fig. 1) over a distance of 30m from the TSA shaft, Figure 2. At this stage none of the level 10 struts had been installed.

The principle of the earth support system can be well understood by considering horizontal equilibrium of forces below the lowest level of installed bracing: For excavations in low permeability clays, there is minimal migration of pore water during the timeframe of construction and hence, the clay undergoes undrained shearing at its in-situ water content. Assuming that the wall translates as a rigid body, the limiting horizontal stresses can be estimated from Rankine earth pressure theory. To a first approximation, the net driving pressure (difference between total active and passive earth pressure) on the wall, $\Delta p \approx (\gamma H - 4s_u)$, where γ is the average total unit weight of the overburden soils, H is the cur-

rent excavation depth and s_u the undrained shear strength of the clay (below the excavated grade). For cases where $\Delta p > 0$ (i.e., $\gamma H > 4s_u$ – which commonly occurs for deep excavations in soft-medium clays), the wall must transfer the net earth pressure forces to the overlying bracing system and/or span between the bracing system and an underlying bearing layer (such as the Old Alluvium, Fig. 1). For the cut-and-cover sections of the Circle Line contract C824, the JGP rafts have been included to increase the shear strength of the materials below the excavated grade and hence, increase the available passive resistance. The actual design of the earth support system was based on non-linear finite element methods which simulate the mobilization and redistribution of the earth pressures, flexure of the wall and strutting system at each stage of the excavation.

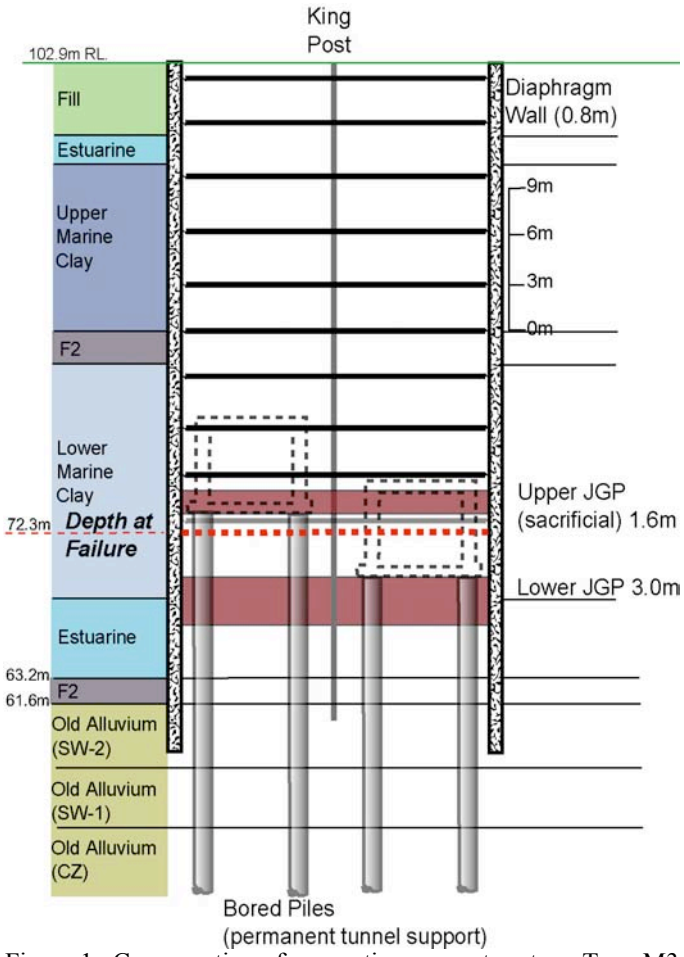

Figure 1. Cross-section of excavation support system, Type M3
(soil profile is based on borehole ABH-32)

2 SITE CHARACTERIZATION AND SOIL PROPERTIES

Figure 2 shows the locations of the pre- and post-tender boreholes (M and ABH series, respectively), that were used to establish the site stratigraphy for the cut-and-cover tunnel sections adjacent to the TSA shaft. The site is located on the west bank of the Kallang River south of Nicoll Highway in an area of reclaimed land. The Merdeka bridge, Figure 3, was constructed in 1956 (Hollis-Bee, 1956) following reclamation of the area between Beach Road and Nicoll Highway in the 1930's and 1940's. Further reclamation south of Nicoll Highway was not completed until 1976. The aerial photo from 1969 confirms that the TSA shaft and adjacent sections of the cut-and-cover tunnels (Type M3) are located beneath the land that was reclaimed during the 1970's. The characteristic soil profile includes 4.5–5.0m of fill underlain by 30–35m of Kallang formation soil deposits and the Old Alluvium. The engineering geology of these main soil units has been extensively documented by Pitts (1983, 1984). The underlying Old Alluvium is generally assumed to date from the early Pleistocene and was formed principally as terrace deposits from a large braided river system that covered much of South East Asia

(Gupta et al., 1987). Erosion of these deposits produced a network of deep paleo-channels within the Old Alluvium beneath Singapore (Pitts, 1983; Davies, 1984).

The paleo-channels are infilled with more recent units of the Kallang formation. Bird et al. (2003) have recently reviewed the age and origins of the Kallang soil deposits based on the history of sea level changes that have occurred during the quaternary period. The formation includes two main units of Marine clay that were formed when the Straits of Singapore were inundated, while transitional units (estuarine, E; and fluvial, F) were formed during periods when the sea level was more than 25m below its present level. According to Bird et al., 2003), the Lower Marine Clay (LMC) dates from the last interglacial period (approximately 120,000 years ago), while the Upper Marine Clay (UMC) is a holocene deposit (formed less than 10,000 years ago).

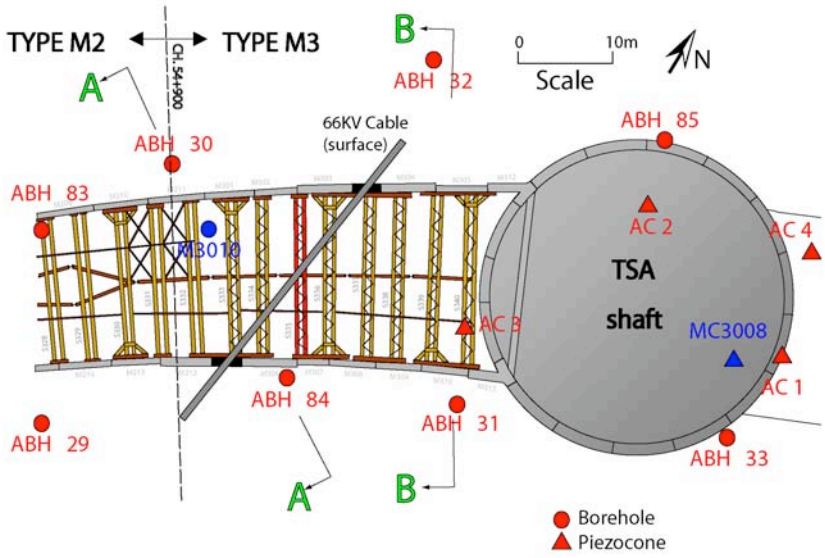

Figure 2 Plan showing location of diaphragm wall panels, 9th level strutting system and site investigation

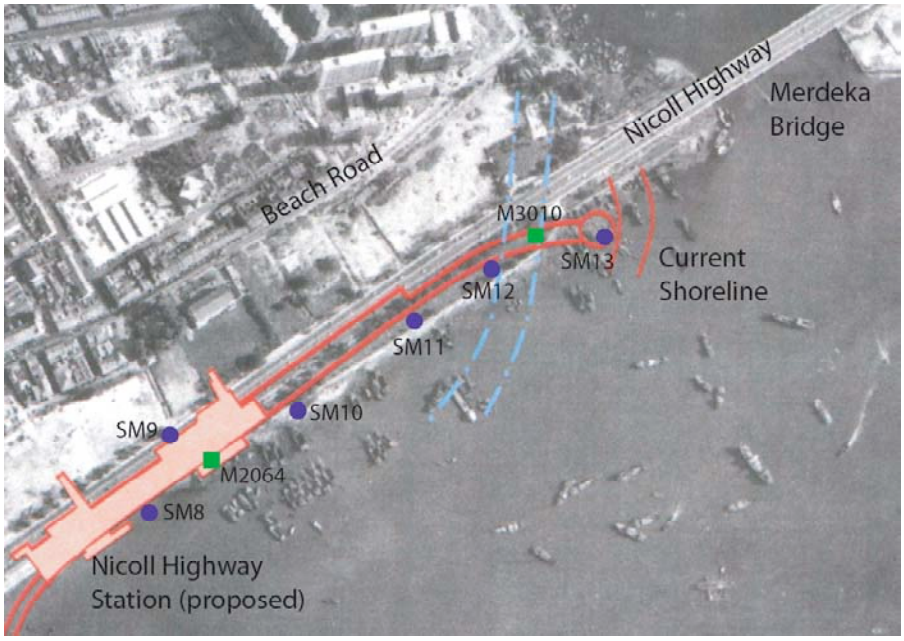

Figure 3. Aerial photo of project site in 1969

For practical purposes (e.g., estimation of undrained shear strength) there is little to distinguish the lower Estuarine and Marine clay units of the Kallang formation (both have plasticity indices, I_p = 35-55%, while the Estuarine has a slightly higher liquid limit, w_L = 70-100% than LMC, w_L = 65-80%). However, it is more difficult to define the interface between the lower Kallang units (which include transitional fluvial units of sands and clays, F1 and F2) and the more weathered Old Alluvium. At the C824 site, most of the Old Alluvium is classified as very dense silty sands transitioning with depth to

very stiff to hard, silty clay. The SPT blowcount increases markedly with depth in the Old Alluvium, ranging from N = 10-20blows/300mm (i.e., blows/foot, bpf) near the upper surface to N > 100bpf typically over a depth of 6m – 10m. In order to simplify the interpretation of the local geology it is convenient to define the top of the Old Alluvium based on measured SPT blowcount, N > 30bpf corresponding to material which can provide adequate toe resistance for the diaphragm wall. Figures 4a and b show elevation contours of the base of the Lower Marine Clay (or Estuarine) unit and top of the Old Alluvium at the C824 site (the ground surface is level at 102.9m RL across the site). There is a well defined channel in the Old Alluvium (Fig. 4b) which extends in a North-South direction across the line of the cut-and-cover tunnels and reaches a maximum depth of 42m close to the TSA shaft. At this same location the Lower Marine Clay extends to a depth of approximately 40m. The Old Alluvium rises progressively moving westwards along the tunnel alignment (types M3 and M2), while the Marine Clay remains deeper along the southern side of the tunnels. More detailed observations of the borings indicate transitional fluvial sand units (F1) between the Old Alluvium and Marine Clay on the North side of the tunnels, and fluvial clay units (F2) on the South side.

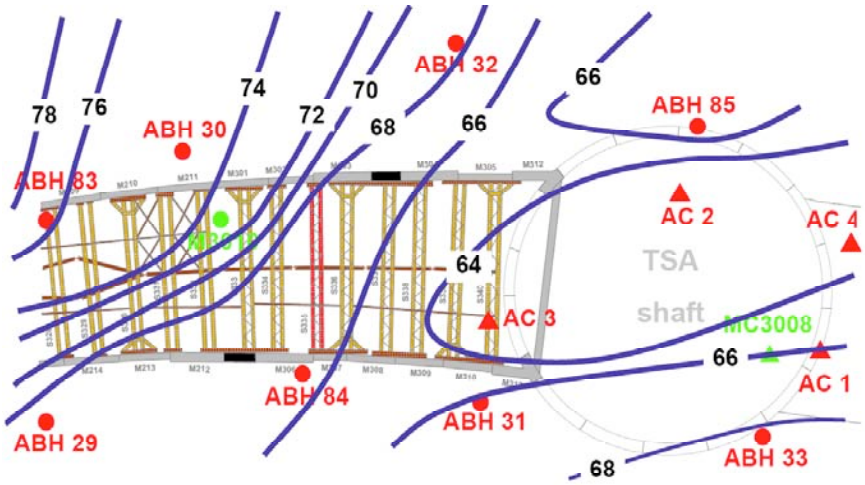

a) Contours of base of Lower Marine Clay (m RL)

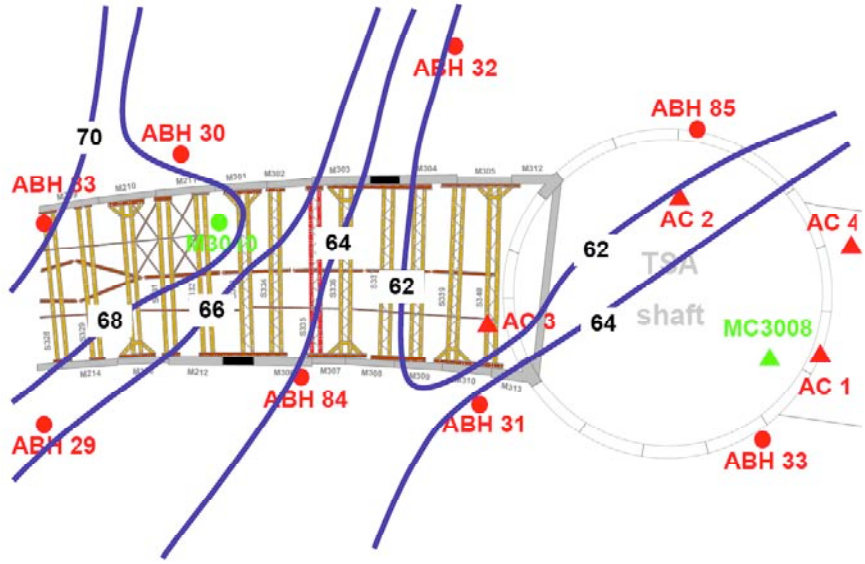

b) Contours showing top of Old Alluvium (N > 30bpf)

Figure 4. Elevation contours derived from pre- and post-tender borehole data

The elevation contours affect the construction of the lateral earth support in two key respects: i) The installation depth of diaphragm wall panels should ensure adequate embedment in the Old Alluvium to achieve toe fixity. The original intent of the design was to achieve 3m embedment within the Old Alluvium (Fig. 1). However, construction records show that the individual panels of the diaphragm wall were actually installed to specified design elevations rather than embedment requirements, Figure 5. Indeed, several panels have embedment depths less than 1m within the Old Alluvium (with N > 30bpf). ii) Continuity of the JGP raft depends on achieving a specified diameter for each the individ-

ual jet grout piles. Field tests in the Upper Marine Clay were used to select the jetting parameters to achieve 2m diameter jet grout columns. The columns will be much smaller if jetting is carried out within stronger layers such as the fluvial deposits and weathered Old Alluvium below the Marine Clay. There were no systematic records of the installed elevations of the JGP layers at the site. According to the design elevations, the lower JGP is installed below the Marine Clay units on the North Wall west of panel M303 and is likely to be discontinuous for sections at the boundary between design sections M2 and M3 (Fig. 2).

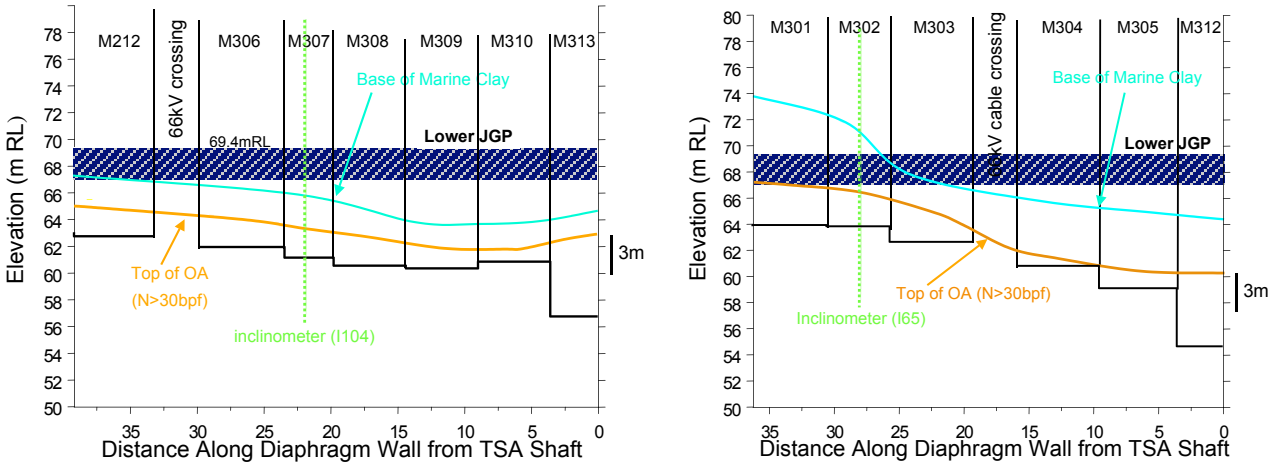

a) South diaphragm wall b) North diaphragm wall

Figure 5. Summary of as-built diaphragm wall panel embedment in M3 area

A series of piezometer installations provided limited data for interpreting the pore pressures within the Marine Clay and Old Alluvium units prior to the start of construction. The groundwater table in the Fill ranges from 100.0mRL – 100.5mRL, while data from boreholes MC3010 and M2064 (Figs. 2, 3) indicate a small excess piezometric head, H = 102m – 103mRL below the Marine Clay. Ground surface settlements were also monitored along the alignment (SM, Fig. 3) over a period of about 15 months (June 2000 – October 2001). The majority of these markers are located close to the 1969 shoreline and measure settlements less than 10mm over the monitoring period, Figure 6. However, settlements of more than 50mm have been measured at points located below the more recent fill (notably SM13). These data suggest the possibility of on-going consolidation within the Marine Clay almost 30 years after land reclamation. The reference in situ vertical effective stress profile, σ'_{v0}, used throughout this paper is based on the assumption of a constant piezometric H = 103m throughout the LMC and OA units.

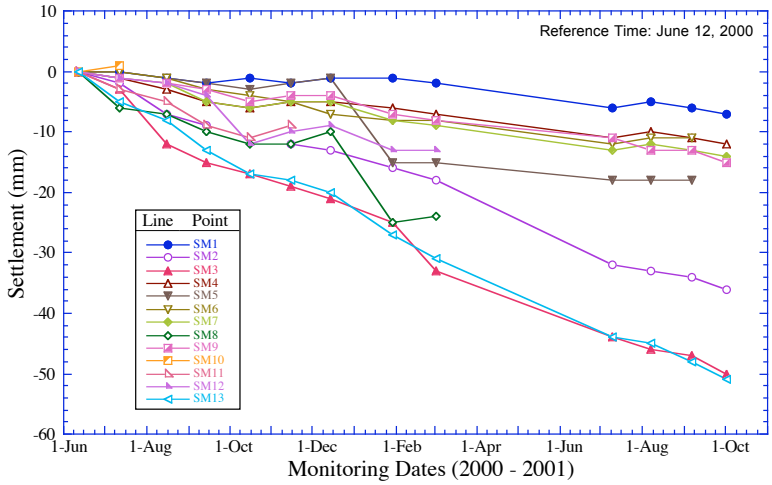

Figure 6. Ground surface settlements measured prior to construction

The design of the temporary lateral earth support system was based on a table of geotechnical design parameters (GIM, August 2001). This table includes the unit weights, K_0 coefficients, hydraulic conductivities, k, elastic moduli, E, and both the Mohr-Coulomb (drained) effective stress strength pa-

rameters (c', ϕ') and undrained shear strength profiles, $s_u(z)$ (for all except the F1 unit) for all of the main soil units and JGP layers. Many of these parameters were based on prior experience (e.g., Bo et al., 2003; Tan et al., 2003; Chiam et al., 2003; Li & Wong, 2001). For example, the design elastic moduli, E [kPa] = $400s_u$ and 2000N in the low permeability Kallang and Old Alluvium units, respectively. The critical parameters for design purposes are the undrained shear strength profile of the Marine Clay, strength parameters and drainage conditions in the Old Alluvium. There are also significant uncertainties in evaluating the properties of the JGP rafts. Although UCS tests on core samples measure strengths much higher than those assumed in design, the mass performance of the raft depends on the continuity between individual jet grouted piles.

2.1 Marine Clay

There were three main sources of undrained shear strength data for the Marine Clays; 1) undrained triaxial shear tests (CIU type, with $K_0 = 1.0$), 2) in situ field vane shear tests, and 3) continuous piezocone penetration resistance data (these data were apparently not considered in GIM, 2001). Although the CIU tests were used to define the drained effective stress strength parameters (c' = 0kPa and ϕ' = 22° and 24° for the Upper and Lower Marine Clay, respectively), they are not a reliable source of information on the in situ undrained strength ratio, s_u/σ'_v (which is affected significantly by the in situ K_0 condition). There was a large scatter in the field vane data, s_{uFV}, which included some very low measurements of undrained shear strengths in the LMC unit. The interpretation of these data is further complicated by the practice of selecting correction factors in estimating design strengths (i.e., the design strength, $s_u = \mu s_{uFV}$, where the correction factor $\mu[I_P]$ was first proposed by Bjerrum, 1973).

Piezocone penetration records provide a more reliable source of information on the undrained shear strength profile in the low permeability clay units. The undrained strength can be correlated to the net tip resistance, $(q_T-\sigma_{v0})$, through an empirical cone factor, N_{kT}:

$$s_u = (q_T - \sigma_{v0})/N_{kT} \qquad (1)$$

where q_T is the measured cone resistance (corrected to account for differential pore pressures acting around the surface of the conical tip), and σ_{v0} is the total overburden pressure.

The cone factor is best estimated through empirical correlations with reference measurements of undrained shear strength from (high quality) laboratory laboratory tests measured in different modes of shearing (triaxial compression, triaxial extension and direct simple shear). Tan et al. (2003) proposed $N_{kT} = 12$ for the Marine Clay based on correlations with laboratory tests at two other sites in Singapore, while the various experts contributing to the COI assumed $N_{kT} = 12 - 14$. These values are well within the range of empirical correlations presented by Lunne et al. (1997). Figure 7 compares the undrained strength profiles interpreted from 4 piezocone tests in the M3 area assuming $N_{kT} = 14$. The tests show very consistent agreement in both the Upper and Lower Marine Clay units, while AC-3 gives substantially high shear strengths than the other three for the UMC layer.

The undrained shear strength ratio of the normally consolidated Marine Clay is usually assumed to be; $s_u/\sigma'_{v0} = 0.21$ (for the direct simple shear mode of shearing; Tan et al., 2003). Figure 7 shows that this strength ratio is consistent with the interpreted piezocone strengths at elevations 86 - 94mRL and 75 - 80mRL, based on the estimated profile of the current vertical effective stress (Fig. 7b). However, the data also suggest that the Lower Marine Clay below 75mRL is weaker than this expected strength profile. The interpreted strength at the base of the LMC unit (at 63mRL), s_u = 47kPa, is more than 10kPa less than the undrained shear strength expected for the normally consolidated clay. This behavior can be attributed to one or more of the following factors: i) the Lower Marine Clay should be described has a lower undrained strength ratio than the overlying units. There is no direct experimental basis for this assumption. ii) The Lower Marine Clay is underconsolidated locally (i.e., has not fully consolidated under the 5m fill placed in the 1970's). This implies that the piezometric pressures in the Lower Marine Clay are higher than 103mRL and could explain the surface settlements shown in Figure 6. It also implies that there is no seepage into the underlying Old Alluvium (i.e., there is one way upward drainage within the LMC). iii) Undrained shear strength in the LMC is underestimated using N_{kT} =14. There is no direct basis for refining the selection of N_{kT}, the current choice produces consistent interpretation of the design s_u profile above 75mRL. The GIM (2001) design table assumes that the Marine Clay is normally consolidated below a depth of 15m and hence, potentially overestimates the undrained shear strength by up to 10-15kPa. There were no reliable stress history data obtained from the pre- and post-tender site investigations. However, data from the post-collapse investigations (at boreholes outside the zone of the collapse), Fig. 7b, confirm that the Marine Clay is normally con-

solidated below a depth of 10m, and the transition fluvial unit (F2) is lightly overconsolidated. Figure 7 shows the Authors' best estimate of the undrained strength profile in the M3 area.

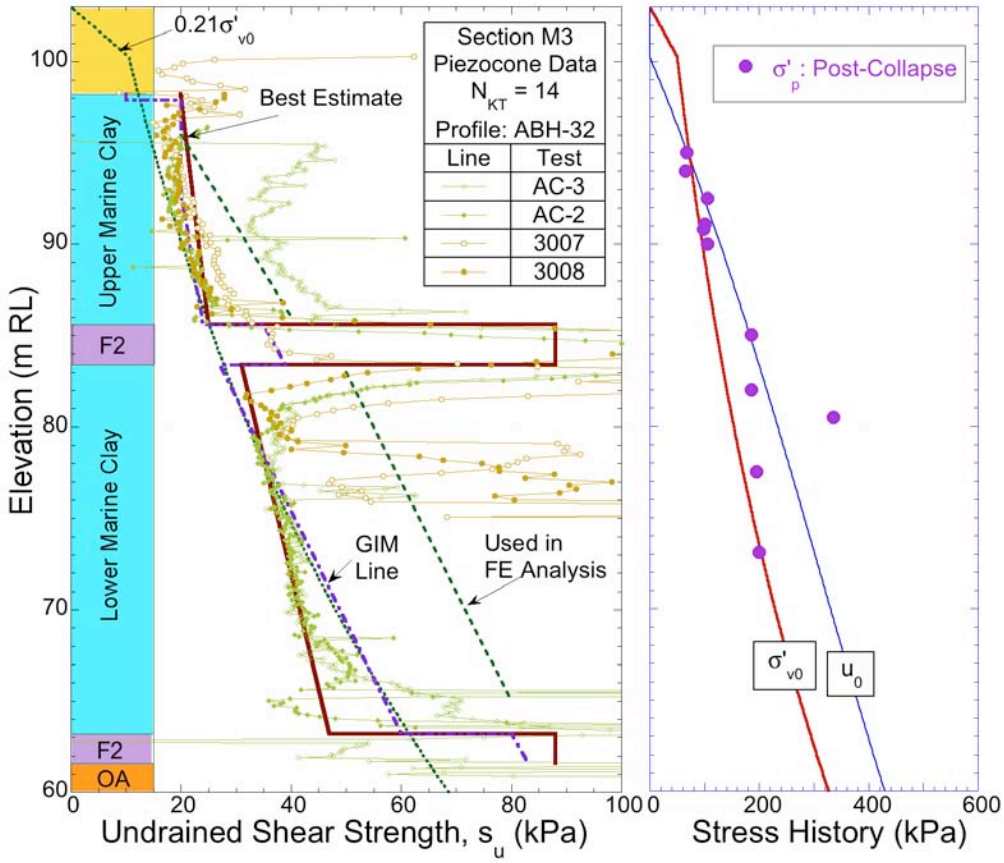

Figure 7. Undrained shear strength of Marine Clay, Section M3

2.2 Old Alluvium

The drainage properties of the Old Alluvium have important practical implications in the design of the lateral earth support system. The upper 5-10m of the Old Alluvium are weathered (zones W, SW-2 and SW-1) and generally classified as silty sands or silty clays (although there are locations which include hard clays layers). These materials are generally more permeable than the underlying intact material (cemented zone, CZ), or the overlying Marine Clay ($k = 10^{-9}$m/sec; GIM, 2001). The original table of design parameters quoted values of permeability, $k = 5x10^{-7}$ and $5x10^{-8}$m/sec for the weathered OA layers and intact CZ layer, respectively. In comparison, Li and Wong (2001) report $k = 10^{-9} – 10^{-10}$m/sec for intact Old Alluvium. Overall, these data suggest that recharge of pore pressures below the base of the excavation depends on lateral seepage and hence, depends on the extent and continuity of the weathered more permeable OA deposits (and overlying fluvial sands, F1).

The original design assumed that the weathered OA layers were free draining materials with pore pressures (below the base of the excavation) controlled by the excavated grade elevation. This condition can only be achieved in practice if the diaphragm walls form a hydraulic cut-off (i.e., extend into the intact OA material) and relief wells are installed through the JGP to reduce uplift pressures in the weathered OA. In practice, the embedment of the diaphragm walls is not sufficient to ensure hydraulic isolation below the base of the excavation (cf. Fig. 5). However, the assumption of free draining conditions is highly unrealistic and would imply no reduction in the pore pressures below the base of the excavation (i.e., there is full recharge). This condition would lead to premature basal failure through hydraulic uplift.

Our own investigations suggest that very little migration of pore water is likely to occur within the time frame of the excavation and hence, it is more reasonable to assume undrained shearing conditions within the weathered OA (the undrained shear strength of the Old Alluvium can then be estimated using empirical correlations, s_u(kPa) = 5N(bpf) as proposed by GIM, 2001). According to this scenario,

significant reductions in pore pressures should occur in the Old Alluvium. The magnitude of pore pressure change can be estimated using the well known Skempton pore pressure parameters, A and B:

$$\Delta u = B\Delta\sigma_3 + AB(\Delta\sigma_1-\Delta\sigma_3) \quad (2)$$

where $\Delta\sigma_1$ and $\Delta\sigma_3$ are the changes in (major and minor principal) total stresses due to the excavation (the ratio $\Delta\sigma_3 / \Delta\sigma_1$ will depend on the depth to width of the excavation, for a very wide excavation 1-D generate $\Delta\sigma_3 = 0$ and $\Delta\sigma_1 = \Delta\sigma_v$). For saturated soils, it is generally assumed that B = 1.0 while the parameter A depends on soil shear properties. For elastic unloading, A = 0.5, hence the change in pore pressure expected beneath the center of the excavation $\Delta u \leq 0.5\Delta\sigma_v$.

Partial drainage within the Old Alluvium can be evaluated directly by monitoring pore pressures within the Old Alluvium. Unfortunately, there was only one piezometer installed beneath the excavation within the weathered OA material in the M3 area (GWV-24 located close to the north diaphragm wall at 64mRL). This device measured $\Delta u = 0.25 – 0.30\Delta\sigma_v$ (where $\Delta\sigma_v$ is the 1-D vertical stress relief) for excavation to 82 mRL (i.e, to strut level 6, Fig. 1), but was ineffective thereafter. Finite element simulations of these data are consistent with the assumption of undrained conditions.

3 ANALYSIS OF SOIL-STRUCTURE INTERACTION

3.1 Method and Assumptions

The design of the lateral earth support system for Contract 824 was based directly on results of non-linear Finite Element (FE) analyses using the Plaxis program (v7.2). This program is capable of modeling response of the continuous ground mass (deformations and groundwater seepage) and interactions with the structural support elements (perimeter wall, preloaded cross-lot struts) in two dimensions. At each stage of a simulated construction schedule, the numerical analyses generate information on the bending moments and deflections of the perimeter diaphragm wall, axial strut forces, ground deformations and pore pressures. By representing the complex stress changes within the soil mass during an excavation (arching mechanisms etc.), 2-D FE programs such as Plaxis represent a major in advance in analysis capabilities compared to conventional 1-D (FE) models of support systems (e.g., Wallap, Geosolve, 2002; Kasetsu-5x, CRCRI, 1999). However, effective utilization of these capabilities requires: a) careful specification of boundary and initial conditions (in situ soil stresses and groundwater conditions), b) selection of soil models with appropriate input parameters to represent engineering properties of the pertinent soil layers (shear strength, stiffness parameters and permeability); and c) methods for interpreting and evaluating predictions of the analyses. There also remains a major question regarding the appropriate use of finite element methods in the design of excavation support systems particularly in the definition of 'worst credible' or 'moderately conservative' ground (soil and groundwater properties) and loading conditions (as discussed by Simpson & Yazdchi, 2003).

The default mode of calculation used by Plaxis treats soil as a two phase medium comprising the soil skeleton and interstitial pore water (it is also possible to model single phase, 'non-porous' materials). The Plaxis program follows conventional geotechnical design calculations which assume simplified drainage conditions (i.e., flow of groundwater) within soil layers. Low permeability clays are treated as undrained materials (i.e., there is no migration of pore water within the skeleton over the time frame of interest), while more permeable sands are considered fully drained (i.e, pore pressures are always in a steady state condition - as groundwater flow can occur rapidly relative to the timeframe of interest). Time dependent deformations due to consolidation (or creep) can also be simulated in Plaxis. Although consolidation can contribute significantly to the interpretation of ground settlements around a braced excavation in soft clay (i.e., in the interpretation of field performance), the current design appropriately ignores consolidation in the design of the excavation support system.

Plaxis offers a range of constitutive models of varying complexity to characterize the deformation and shear strength properties of soil layers. The default model is referred to as a linearly Elastic-Perfectly Plastic model (EPP) – which has four basic input parameters: The pre-failure stiffness of the soil is characterized by two elastic properties (E' , Young's modulus; and ν', Poisson's ratio) while the shear strength is described by the conventional Mohr-Coulomb criterion. The undrained shear strength of the clay can be represented either using A) effective stress, strength parameters (c', apparent cohesion; and ϕ', internal friction angle); or B) undrained shear strengths (c' $\rightarrow$ s_u; ϕ' = 0°). These ap-

proaches are referred to as Methods A and B in the COI report (COI, 2005) and the subsequent discussions.

The EPP model is almost universally accepted as the base level representation of soil behavior suitable for design. More advanced models (notably 'Hardening Soil', Schantz et al., 2000) are also available within Plaxis and can describe more realistically the non-linear stress-strain properties of real soils. Although these models can improve the predictive capability of FE analyses (this is especially helpful in interpreting field performance measurements), they introduce additional material parameters and require more extensive calibration of soil properties. Although the use of such models would certainly have been justified based on the size and importance of this project, it is clearly beyond the scope of soil data available from the (pre- and post-tender) site investigation that was actually carried out.

According to the EPP model, there is no change in mean effective stress during undrained shearing (i.e,. there are no shear-induced pore pressures and hence, $\Delta u = \Delta\sigma_{oct}$ where $\sigma_{oct} = 1/3[\Delta\sigma_1 + \Delta\sigma_2 + \Delta\sigma_3]$ is the mean total stress). For undrained triaxial compression tests with $\Delta\sigma_3 = 0$, A = 0.33 (eqn. 2), while all undrained plane strain, shear modes are characterized by A = 0.5. Figure 8 illustrates the effective stress path (A'-B') for undrained plane strain shearing. It is clear that the undrained shear strengths according to Methods A and B are interrelated as follows:

$$s_u = c'\cos\phi' + 1/2(\sigma'_1+\sigma'_3)\sin\phi' \qquad (3a)$$

Assuming that the initial state of stress is defined by K_0 conditions in the ground, then Method A implies that the undrained strength ratio is given by:

$$s_u/\sigma'_{v0} = (c'/\sigma'_{v0})\cos\phi' + 1/2(1+K_0)\sin\phi' \qquad (3b)$$

where σ'_{v0} is the initial vertical effective stress at a given depth in the ground.

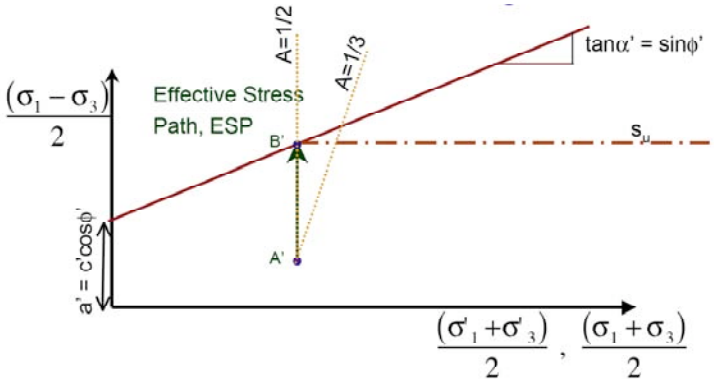

Figure 8. Effective stress path for undrained plane strain shearing using EPP (Mohr-Coulomb) soil model

There is extensive empirical information relating the undrained shear strength to the stress history of sedimentary clays. The most widely used correlations (e.g., SHANSEP; Ladd and Foott, 1974) relate the undrained strength ratio s_u/σ'_v to the overconsolidation ratio, $OCR = \sigma'_p/\sigma'_v$, where σ'_p is the vertical pre-consolidation pressure. For example, Figure 9 shows an expected correlation for the Singapore Marine Clay based on $S = s_u/\sigma'_v = 0.21$ for the normally consolidated case (OCR = 1.0; Fig. 7). The Figure also shows the undrained shear strength obtained in plane strain analyses using Method A with the effective stress strength parameters that were used in the original design (i.e., c' = 0kPa and ϕ' = 22°, 24° for UMC and LMC, respectively), together with well known empirical correlations for K_0. It is clear that Method A overestimates the undrained shear strength for normally and lightly overconsolidated clay (OCR < 2), but is generally conservative at higher OCR.

The practical consequence of using the EPP with Method A is most clearly seen in Figure 7 which shows the undrained shear strength profile that was implicitly used in the finite element design analyses. The undrained shear strength is much larger than the original design line (GIM, 2001), particularly in the Lower Marine Clay. In contrast, Method B uses the undrained strength profile directly in the finite element analyses and is certainly the most reliable way to use the EPP model for simulating undrained behavior of clays for Contract 824. The potential disadvantage of Method B is that the shear strength is no longer a function of effective stress and hence, changes in shear strength due to consolidation (partial drainage) are no longer represented. This limitation is mute for design calculations that assume undrained conditions (through the timeframe of an excavation), but can be a serious limitation when modeling problems where consolidation deformations are significant.

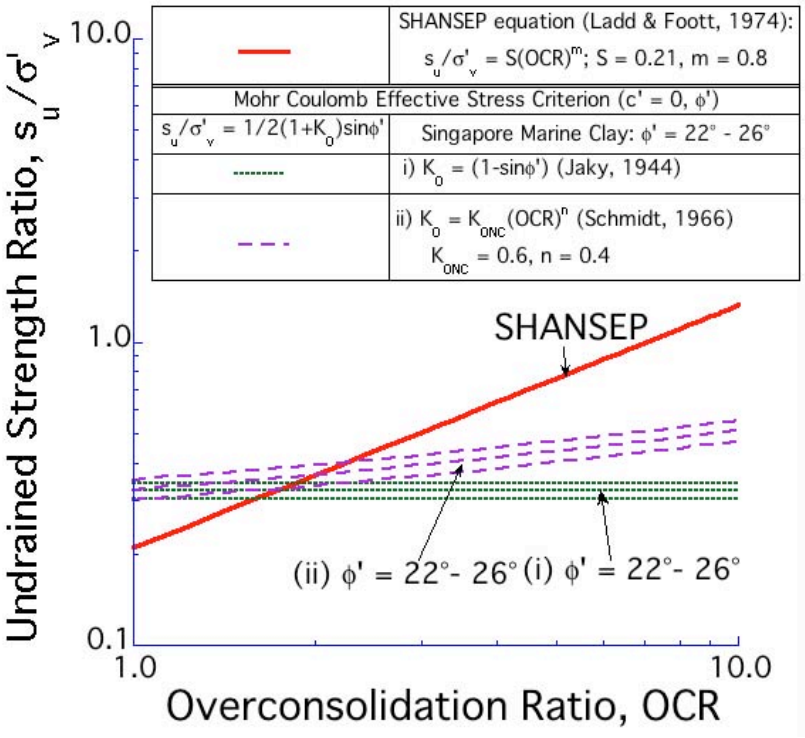

Figure 9. Comparison of the undrained strength ratio for the Marine Clay using Method A with empirical correlations based on SHANSEP

3.2 Effect of Analysis Method and Undrained Strength Profile on Design

A series of finite element simulations have been carried out (using Plaxis v8.2) to investigate the role of the analysis method (A vs B) and selection of undrained strength profile on the type M3 design of the temporary lateral earth support system. This section illustrates results from 4 of these calculations with characteristic properties as follows:

- A[NLC] is a calculation that reproduces the original design assumptions. The undrained shear strength of the Marine and Estuarine Clay units are based on the use of effective stress strength parameters (c', ϕ') provided by GIM (2001) according to Method A. The corresponding undrained shear strength profile is shown in Figure 10. The weathered Old Alluvium (SW-2) is assumed to be free draining with pore pressures defined by the current excavation grade elevation (as per the original design). The analyses also uses the initial K_0, soil stiffness and JGP properties prescribed by GIM (2001).
- B[GIM] uses Method B (s_u, ϕ' = 0°) to represent the undrained strength profile for the Marine and Estuarine clay layers.
- GIM* also uses Method B, but makes three amendments that are consistent with our interpretation of local ground conditions: i) the lower Estuarine unit has the same undrained strength profile as the Lower Marine Clay (s_u/σ'_v = 0.21); ii) the weathered Old Alluvium (SW-2) is undrained with strength properties related to the SPT data according to GIM (2001); and iii) the lower JGP was constructed to a design thickness of 2.6m (as compared to 3.0 assumed in the design analyses).
- EBC makes one further modification to the previous case (GIM*), by introducing an improved estimate of the undrained strength profile in the Lower Marine Clay (EBC; Fig. 10) based on the interpretation of piezocone data presented in Figure 7.

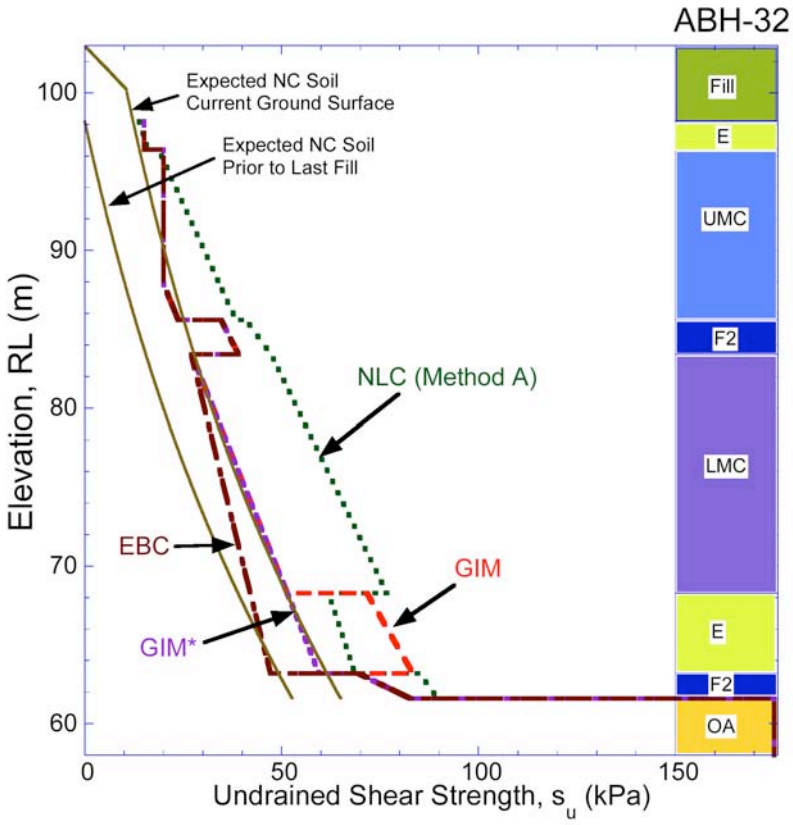

Figure 10. Undrained strength profiles used in FE simulations for Type M3 excavation support system

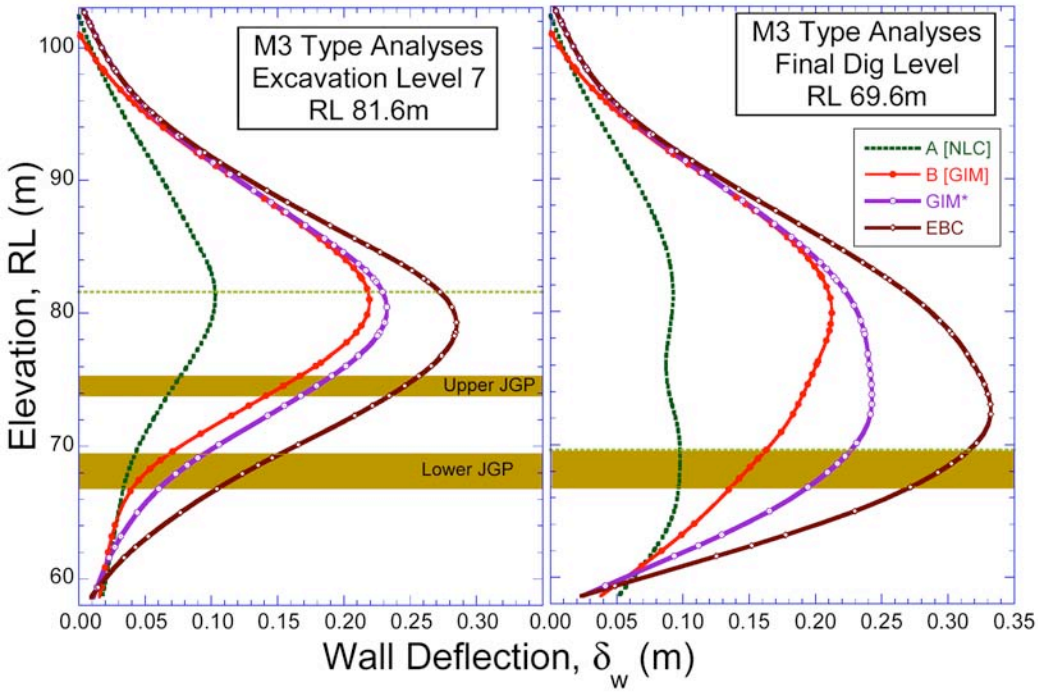

Figure 11. Effect of undrained shear strength profile on wall deflections for Type M3 excavation support system

Figures 11a and b compare predictions of the lateral wall deflections from these analyses for excavation to the 7th level struts (81.6 mRL) and final formation level (69.6 mRL), respectively. The results show the following:

Wall deflections computed by Method B are approximately a factor of 2 larger than those computed using Method A. There is a similar difference in the magnitude of the bending moments computed from the two analyses. The two Methods predict very similar deflection mode shapes at level 7 (Fig. 11a) with maximum deflections occurring at 81m RL. However, quite different mode shapes develop

as the excavation proceeds to level 10 (Fig. 11b). Both analyses predict minimal change in the maximum wall deflection (100mm and 210mm for A and B, respectively) for excavations below level 7. This behavior can be understood through further comparison of results from B[GIM] and GIM*. These two cases show very similar wall deflections at level 7. However, GIM* predict a significant increment in wall deflection below 81mRL for excavation to the final formation. This behavior reflects the refinement in the selection of undrained strength properties in the lower Estuarine and Old Alluvium (SW-2) layers and the full mobilization of the resistance of the lower JGP.

The EBC case can be interpreted as a worst credible interpretation of the undrained shear strength profile as it implies underconsolidation of the Lower Marine Clay. Figure 11a shows that the EBC profile generates an additional 50mm of wall deflection at level 7 and up to 90mm additional deflection at the final formation elevation. These results confirm that small variations in the undrained shear strength within the LMC (and lower E) layers can produce significant changes in computed wall deflections.

The same set of analyses have been used to investigate the mobilization of the passive resistance within the JGP layers. Figure 12a compares the predicted axial force (F_x) in the upper and lower JGP layers with the design load capacities using Methods A and B as functions of the excavation depth. (with formation elevation for levels 2-9). The computed loads are compared with the design capacity based on the theoretical passive earth pressures stresses (JGP has design s_u = 300kPa). The Figure presents results for analysis case A (2.6m thick lower JGP) and B[GIM*]. The results show very clearly that Method B mobilizes the passive resistance of the JGP layers at much higher formation elevations than Method A. For the lower JGP, Method B predicts that the design capacity becomes fully mobilized for excavation below level 6, while Method A calculations show this condition only occurs below level 9.

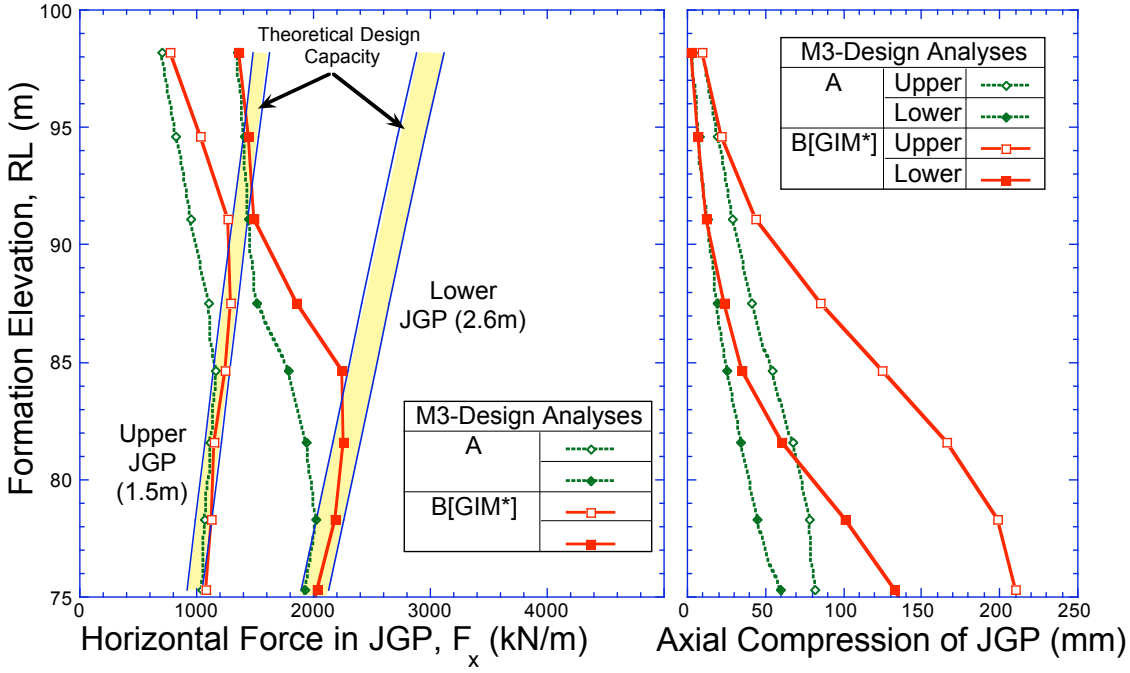

Notes: The theoretical horizontal passive earth pressure, $\sigma_h = \sigma_v + xs_u$, where x= 2.0 – 2.3 depending on the wall adhesion.

Figure 12. Effect of analysis method on mobilization of passive capacity of JGP layers

Mobilization of the passive resistance of the JGP layers is correlated with the axial compression and hence, can be conveniently compared to measurements of wall deflection. Figure 12b presents the corresponding axial compression of the upper and lower JGP layers computed using Methods A and B[GIM*]. Method B shows significant deviation from Method A predictions of axial compression below level 3 for the Upper JGP and below level 6 for the lower JGP layers, respectively.

Figure 13 summarizes the maximum computed loads in strut levels 6, 7 and 9 during the excavation for the four analysis cases described above (level 8 was not included as the strut was designed for maximum loads occurring during subsequent tunnel construction). These calculations incorporated the theoretical axial load and bending moment capacities of the struts and diaphragm wall used in the

Type M3 design. Method B predicts higher loads in strut levels 6 and 7 than Method A, due to differences in the undrained shear strength of the Marine Clay units. However, ironically the level 9 load is slightly higher for Method A than for Method B. This result is apparently due to compensating errors in the undrained hear strength assumed in the lower Estuarine unit (see su profiles for A[NLC] and B[GIM] in Fig. 10). The computed loads in level 9 (as well as levels 6 and 7) struts increase significantly for the GIM* and EBC analysis cases. The Method B calculations (GIM, GIM*, EBC) all predict yielding of the diaphragm wall for excavation below 81mRL. The calculations for the worst case soil profile (EBC) generate struts loads very close to the design capacity of both level 6 and level 9 struts. The strut load in the level 9 struts is expected to exceed 2000kN/m from all four analysis cases and hence, exceeds the installed capacity of the strut-waler connection.

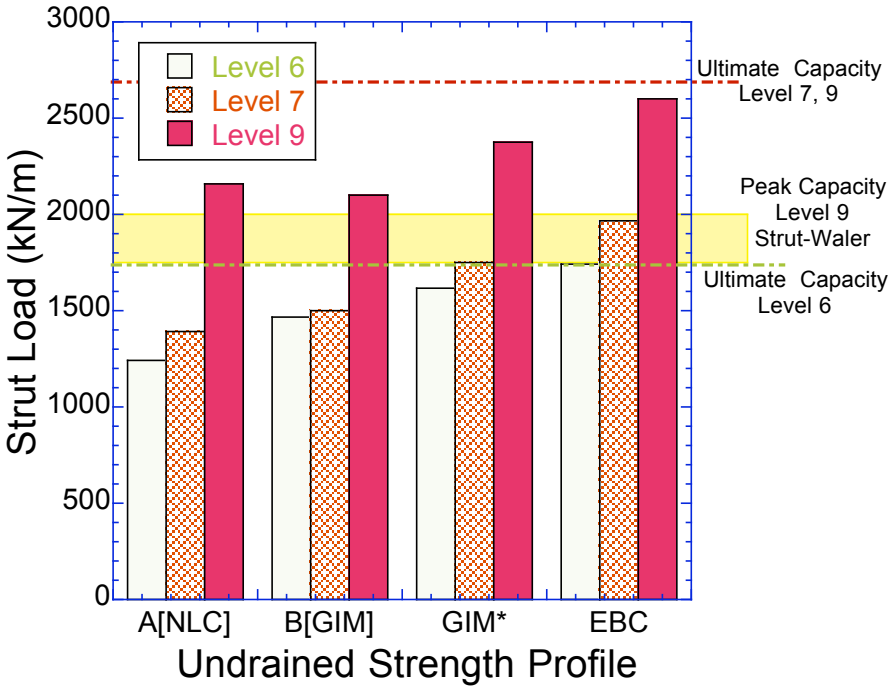

Figure 13. Effect of the analysis method and undrained shear strength profile on computed strut loads

The overall stability of the excavation can be evaluated in Plaxis using the c-ϕ reduction technique (Brinkgreve & Bakker, 1991). This method obtains directly the partial factor of safety on soil shear strength ('mobilization factor'):

$$FS = \tan\phi'/\tan\phi'_{red} = c'/c'_{red} = s_u/s_{ured} \quad (4)$$

where ϕ', c' and s_u are the input shear strength parameters, and the subscript 'red' refers to reduced values of these parameters necessary to generate a failure mechanism in the FE model.

According to BS8002, the partial factors on the shear strength parameters, FS = 1.2 for parameters c' and tanϕ', while FS = 1.5 for s_u. The results for Method A show FS = 1.14 for excavation to the final formation level, while all method B analyses generate FS < 1.3 for excavation to the level 9 struts (the worst case EBC profile produces FS = 1.12). No overall stability calculations were presented for the original design.

None of the preceding calculations have included the actual/installed capacity of the strut-waler connection at level 9. Our investigations found that collapse of the Nicoll Highway occurred due to the inability of the excavation support system to redistribute loads after failure of the 9th level strut-waler connection. Figure 14 illustrates the role of the analysis method on the ability of the support system to redistribute loads after failure of the 9th level of struts. The analyses simulate excavation down to the depth reached on April 20th 2004 (72.3 mRL) and then evaluate the stability if the 9th level of struts is removed (i.e., full softening of the strut-waler connection). Figure 14a shows the wall deflections and strut loads from Methods A and B[GIM], while Figure 14b shows the bending moment envelope prior to failure of the 9th level waler and the subsequent bending moment diagrams. It should be noted that Method B generates larger bending moments in the preceding stages of excavation than Method A, exceeding the design wall capacity and enabling potential hinge formation (between 8

8mRL and 78 mRL on the excavated side and at RL 68 mRL on the retained side). Removal of the 9th level strut causes the following events:

1. Both Methods A and B predict formation of two plastic hinges (RL 73m and RL 79m) with large wall toe rotation.
2. Method B predicts failure of the 8th level strut (capacity 3220kN/m) and initiates collapse within the soil mass. All three of the Method B analyses (GIM, GIM* and EBC) show that it is not possible to re-distribute loads after removal of the 9th levels struts.
3. In contrast, Method A computes loads below the theoretical capacity of strut 8 and predicts a mobilization factor, FS = 1.16 within the soil mass. Therefore, Method A would predict successful redistribution following failure of the 9th level strut-waler connection.

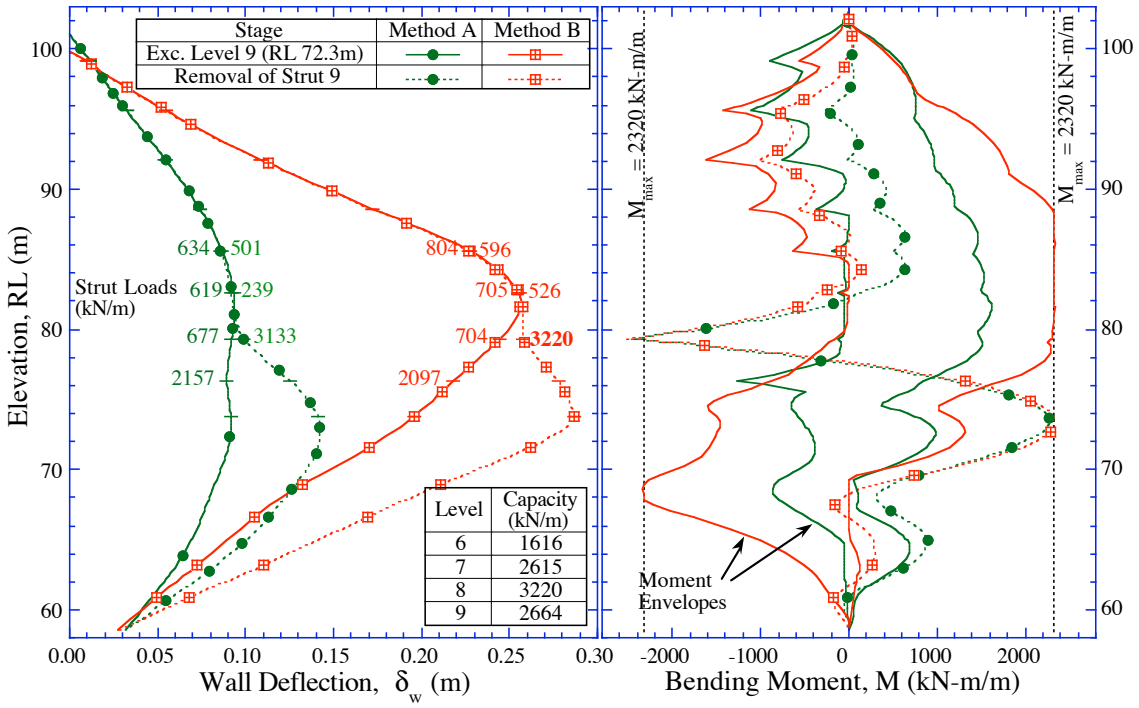

Figure 14. Effect of analysis method on load re-distribution following failure of the 9th level strut-waler connection

4 CONCLUSIONS

The construction of the Circle Line Stage 1 in Contract 824 adjacent to the Nicoll Highway involved the deepest cut-and-cover excavations in soft marine clay attempted to date in Singapore. In the M3 failure area, the excavation support design included ten levels of preloaded cross-lot bracing together with two rafts of jet grouted piles (JGP). The latter constitutes a specialized ground improvement technology used successfully in prior deep excavation projects in Singapore. Use of relatively thin JGP layers (less than 3m thick) and the specification of a sacrificial upper JGP layer were novel aspects of the excavation support system.

The collapse occurred in an area where land was reclaimed in the 1970's with approximately 5m of fill. The site includes deep deposits of Marine clays that extend to a depth of 40m, infilling a buried channel in the underlying Old Alluvium which bisects the tunnel alignment in the M3 area. The undrained shear strength profile in the Marine Clay is best interpreted from piezocone records. These data confirm that the upper units of Marine Clay are normally consolidated and can be described by the design undrained strength ratio, $s_u/\sigma'_v = 0.21$. The undrained shear strength of the Lower Marine Clay (and lower Estuarine) appear to be lower than this normally consolidated strength line. It is likely that these units are still underconsolidated due to reclamation. This result is consistent with local measurements of surface settlements prior to construction and implies that the underlying Old Alluvium is effectively impermeable.

A detailed re-evaluation of the local stratigraphy shows that some of the diaphragm wall panels installed the M3 area had toe embedment depths substantially less than the 3m intended in the design.

The design of the excavation support system was based on results of relatively sophisticated 2-D, non-linear finite element analyses, using linearly elastic-perfectly plastic soil models (EPP or Mohr-Coulomb) to represent the sear behavior of the soils and JGP layers. The original design calculations assumed effective stress strength parameters (c', ϕ') to represent the behavior of low permeability clay units. This approach, referred to as Method A, grossly overestimated the undrained shear strength profile for the normally (or underconsolidated) Marine Clays (Fig. 7). The shear behavior of low permeability, normally or lightly overconsolidated clays should be analyzed by inputting directly the design undrained shear strength profile, $s_u(z)$ (assuming $\phi' = 0°$), Method B. The original design also made erroneous assumptions concerning the interpretation of pore pressures and drainage conditions in the underlying Old Alluvium. The use of Method A in the analyses of soil-structure interaction led to underestimation of the computed diaphragm wall deflections and bending moments (both by a factor of 2). The analyses also underestimated the mobilization of the passive shear resistance in the JGP layers.

Further analyses using Method B show that refinement of the undrained strength profile in the Lower Marine and Estuarine clay (GIM* or EBC profiles) will lead to even higher wall deflections, bending moments and strut forces than expected using the original design parameters. They also imply that failure of the 9th level strut-waler connection would initiate complete collapse of the excavation support system in contrast to Method A, where there is sufficient reserve capacity to enable full load redistribution.

Uncertainties and risks associated with recharge and hydraulic uplift conditions could be mitigated through more widespread monitoring of pore pressures within the Old Alluvium. The mass properties of the JGP layers remain highly uncertain in design, but the in situ performance is readily interpreted through measurements of axial compression that were available in the M3 area.

ACKNOWLEDGMENTS

The Authors are very grateful to their colleagues Brian Bell and Dr Chiew Sing-Ping for elucidating the structural performance of the excavation support system. They are especially grateful to Alison Norrish for her invaluable contributions to this work.

REFERENCES

Bird, M.I., Chang, C.H., Shirlaw, J.N., Tan, T.S. & Teh, T.S. (2003) "The age and origin of the quaternary sediments of Singapore with emphasis on the Marine Clay," *Proc. Underground Singapore, 2003*, 428-440.

Bjerrum , L. (1973) "Problems of soil mechanics and construction on soft clays and structurally unstable soils," *Proc. 8th Intl. Conf. Soil Mechanics and Foundation Engineering*, Moscow, 3, 111-159.

Bo, M.W., Choa, V. & Hong, K.H. (2003) "Material characterization of Singapore Marine Clay at Changi," *Quarterly Journal of Engineering Geology and Hydrogeology*, **36**, 305-319.

Brinkgreve, R.B.J. & Bakker, H.L. (1991) "Non-linear finite element analysis of safety factors." *Proc. 7th Intl. Conf on Comp. Methods & Advances in Geomechanics*, Cairns, Balkema, 2, 1117-1122.

Chiam, S.L., Wong, K.S., Tan, T.S., Ni, Q., Khoo, K.S. & Chu, J. (2003) "The Old Alluvium," *Proc. Underground Singapore, 2003*, 408-427.

COI (2005) "Report of the Committee of Inquiry into the incident at the MRT Circle Line worksite that led to collapse of Nicoll Highway on 2o0 April 2004," Ministry of Manpower, Singapore.

CRCCI (1999) www.civil-eye.com/software/jiban/**kasetsu5x**/index.htm

Davies, R.V. (1984) "Some geotechnical problems with foundations and basements in Singapore," *Proc. Conf. On Tall Buildings*, Inst. Engineers, Singapore, 643-650.

Geosolve (2002) http://www.geosolve.co.uk/wallap1.htm

GIM (2001) Geotechnical Interpretative Memorandum C824/DES/DM/002A, Project Document.

Gupta, G.A., Rahman, A., Wong, P.P. & Pitts, J. (1987) "The Old Alluvium of Singapore and the extinct drainage system to the South China Sea," *Earth Surface Processes and Landforms*, 12, 259-275.

Hollis-Bee, R.J. (1956) "Construction of the bridge," in Opening ceremony: Merdeka Bridge and Nicoll Highway, August 17, 1956, Singapore Government Printing Office.

Ladd, C.C. & Foott, R. (1974) "New design procedure for stability of soft clays," *ASCE Journal of Geotechnical Engineering*, 100(GT7), 763-786.

Li, W.W. & Wong, K.S. (2001) "Geotechnical properties of Old Alluvium in Singapore," *Proc. Journal of the Institution of Engineers*, Singapore, 41(3), 10-20.

Lunne T., Robertson, P.K. & Powell, J.J.M. (1997) Cone penetration testing in geotechnical practice, *Blackie Academic & Professional*, London, UK.

Pitts, J. (1983) "The origin, nature and extent of recent deposits in Singapore," *Proc. Intl. Seminar on Construction Problems in Soft Soils*, Singapore, 1-18.

Pitts. J. (1984) "A review of geology and engineering geology in Singapore," *Quarterly Journal of Engineering Geology and Hydrogeology*, **17**: 93-101.

Plaxis (2003) http://www.plaxis.nl/

Schantz, T., Vermeer, P.A. & Bonnier, P.G. (1999) "The hardening soil model: Formulation and verification," *Beyond 2000 in Computational Geotechnics*, Balkema, Rotterdam, 281-296.

Simpson, B. & Yazdchi, M. (2003) "Use of finite elements in geotechnical limit state design," *Proc. Intl. Workshop on Limit State Design in Geotechnical Engineering Practice*, Eds. Phoon, Honjo & Gilbert, World Scientific Publishing, 25p.

Tan, T.S., Phoon, K.K., Lee, F.H., Tanaka, H., Locat, J. & Chong, P.T. (2003) "A characterization study of Singapore Lower Marine Clay," *Proc. Conf. On Characterization and Engineering Properties of Natural Soils*, Eds. Tan et al., Swets & Zeitlinger, 1, 429-454.